A fast multipole boundary element method for solving the thin plate bending problem

S. Huang, Y.J. Liu*

Mechanical Engineering, University of Cincinnati, P.O. Box 210072, Cincinnati, OH 45221-0072, USA

ARTICLE INFO

ABSTRACT

A fast multipole boundary element method (BEM) for solving large-scale thin plate bending problems is presented in this paper. The method is based on the Kirchhoff thin plate bending theory and the biharmonic equation governing the deflection of the plate. First, the direct boundary integral equations and the conventional BEM for thin plate bending problems are reviewed. Second, the complex notation of the kernel functions, expansions and translations in the fast multipole BEM are presented. Finally, a few numerical examples are presented to show the accuracy and efficiency of the fast multipole BEM in solving thin plate bending problems. The bending rigidity of a perforated plate is evaluated using the developed code. It is shown that the fast multipole BEM can be applied to solve plate bending problems with good accuracy. Possible improvements in the efficiency of the method are discussed.

© 2013 Elsevier Ltd. All rights reserved.

1. Introduction

The boundary element method (BEM) has been applied successfully to solve the thin plate bending problem since the late of 1970s and early 1980s. Many researchers derived the direct boundary integral equation (BIE) formulations for both linear and nonlinear responses [1–11]. Using the Rayleigh-Green identity and the fundamental solution, the biharmonic governing equation of Kirchhoff thin plate theory can be transformed into a direct BIE formulation where there are four boundary variables, that is, the deflection, rotation, bending moment, and Kirchhoff equivalent shear force. Generally, two of them are given from the boundary conditions (BCs) and the other two are to be determined. Therefore, two BIEs are required for the thin plate bending problem: the displacement (deflection) BIE and the rotation (normal derivative) BIE. The first BIE is strongly singular, while the second is hypersingular. All these characteristics resemble those of the BIE formulations for potential, elasticity, Stokes flow, acoustic and elastodynamic problems, except for the fact that the use of the hypersingular BIE together with the singular BIE is a must for the plate bending problem using the BEM.

For the conventional BEM, a standard linear system of equations is formed after the BCs are applied. As the coefficient matrix **A** are usually dense and nonsymmetric, every element of **A** need to be stored. Obviously, the construction of **A** requires $O(N^2)$ operations and computer storage (with N being the number of

equations). If direct solvers are used, such as Gauss elimination, a total of $O(N^3)$ operations are required in the solution of the systems. Even when iterative solvers, such as GMRES, are employed, the computational complexity of the algorithm is still $O(N^2)$. This is why the BEM is inefficient in solving large-scale problems.

In the mid of 1980s, Greengard and Rokhlin [12–14] developed the fast multipole method (FMM) to solve potential problems and simulate particle dynamics that can achieve the efficiencies of $O(N)$ operations and computer storage. Many researchers have applied the fast multipole BEM in many other fields, including elasticity, Stokes flows, acoustics, elastodynamics, and electromagnetics. Comprehensive reviews of the fast multipole BEM research can be found in [15,16] and the details of the FMM implementation with the BEM can be found in [17,18]. Despite of the rapid developments of the fast multipole BEM in solving various problems in the last two decades, there are only a few papers on solving the biharmonic equation with the fast multipole method. Greengard, et al. solved 2-D biharmonic interaction problems [19] and elasticity problems [20] based on the biharmonic equation. They decomposed the biharmonic function into two analytic functions (Goursat's formula) and used contour integrals for evaluating these analytic functions in the complex plane. Gumerov and Duraiswami solved the biharmonic equation in 3-D [21], in which the biharmonic equation is decomposed into two harmonic equations. If the above two approaches are to be used to solve the plate bending problem, the four BCs for a plate in bending will be difficult to be related to the two analytic or harmonic functions in a general setting. According to the authors' best knowledge, plate bending problems have not been attempted using the fast

* Corresponding author.
E-mail address: Yijun.Liu@uc.edu (Y.J. Liu).

multipole method based on the direct BIE formulation in which the BCs can be applied directly in a plate bending problem.

In this paper, we apply the fast multipole method to solve large-scale thin plate bending problems that is based on the biharmonic equation and the direct BIE formulation. First, we briefly review the BIEs for Kirchhoff thin plate theory and the related conventional BEM. Then, we introduce the fast multipole algorithm and the complex notation of kernel functions, expansions and translations of the kernels for thin plate bending problems. Finally, a few numerical examples are given to show the accuracy of the developed fast multipole BEM for thin plate bending problems. Possible improvements to the efficiency of the developed method are discussed to conclude the paper.

2. BEM formulation for thin plate bending problems

For completeness, we briefly review the governing equations and the BIE formulations for the Kirchhoff thin plate bending problem.

2.1. BIEs for the thin plate bending problem

The governing equations and the direct BIE formulations for general thin plate bending problems are well documented in the BEM literature [1–11].

Consider an elastic thin plate with its middle surface occupying a 2-D domain V with boundary S (Fig. 1). In terms of deflection $w(\mathbf{x})$, the biharmonic governing equation is:

$$D\nabla^4 w(\mathbf{x}) = q(\mathbf{x}), \quad \mathbf{x}\in V \tag{1}$$

where $D = Eh^3/12(1-\nu^2)$ is the bending rigidity, E is Young's modulus, ν is Poisson's ratio, h is the thickness, and q is the lateral distributed load. The bending and twisting moments M_{ij} are related to the deflection w by the following relationship:

$$M_{ij} = -D[\nu w_{,kk}\delta_{ij} + (1-\nu)w_{,ij}] \tag{2}$$

where $( )_{,i} = \partial ( )/\partial x_i$ and summation over repeated index is assumed. Index notation is used in this paper for convenience and summation is assumed only for indices i, j and k in the range of 1–2. On boundary S, the bending and twisting moments are given by:

$$\left.\begin{array}{l} M_n = M_{ij}n_in_j = -D[\nu\nabla^2 w + (1-\nu)w_{,nn}] \\ M_{nt} = M_{ij}n_it_j = -D(1-\nu)w_{,nt} \end{array}\right\} \tag{3}$$

where n_i and t_i are the direction cosines of the outward normal n and tangential direction t of boundary S, respectively (Fig. 1). The shear force Q_n and Kirchhoff equivalent shear force K_n are
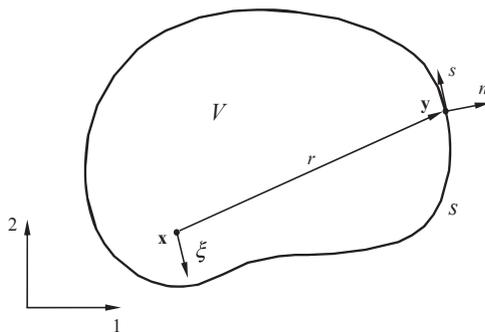

Fig. 1. A domain V with boundary S.

given by:

$$\left.\begin{array}{l} Q_n = M_{ij,j}n_i = -D(\nabla^2 w)_{,n} \\ K_n = Q_n + M_{ns,s} = -D(\nabla^2 w)_{,n} + M_{ns,s} \end{array}\right\} \tag{4}$$

After applying the given boundary conditions, the deflection w of the plate is solved from the governing Eq. (1). Once w is known, the bending and twisting moments and shear forces can be determined by Eqs. (2)–(4).

Governing Eq. (1) can be transformed into a set of integral equations using the fundamental solution $w^*(\mathbf{x},\mathbf{y})$ which is available for thin plate bending problems and satisfies the following equation:

$$D\nabla^4 w^*(\mathbf{x},\mathbf{y}) = \delta(\mathbf{x},\mathbf{y}), \quad \mathbf{x},\mathbf{y}\in R^2 \tag{5}$$

where $\nabla^4( ) = ( )_{,iijj}$ is taken at field point $\mathbf{y}$, $\delta(\mathbf{x},\mathbf{y})$ is the Dirac δ-function representing a concentrated unit force acting at source point $\mathbf{x}$ in the lateral direction, and R^2 is the full 2-D space. The expression of the fundamental solution $w^*(\mathbf{x},\mathbf{y})$ is given as [1, 5–8]:

$$w^*(\mathbf{x},\mathbf{y}) = \frac{1}{8\pi}r^2\log r \tag{6}$$

where $r = |\mathbf{y}-\mathbf{x}|$, and $\mathbf{x}$ and $\mathbf{y}$ are any two points in the 2-D space. The fundamental solution w^* represents the deflection of an infinitely large plate at $\mathbf{y}$ due to the unit force applied at $\mathbf{x}$.

Substituting (6) into (2)–(4), we obtain the corresponding kernel functions for the rotation (or normal slope), bending moment and Kirchhoff equivalent shear force as follows:

$$\theta^*(\mathbf{x},\mathbf{y}) = \frac{\partial w^*}{\partial n} = \frac{1}{8\pi}(1 + 2\log r)r\cos\beta \tag{7}$$

$$M_n^*(\mathbf{x},\mathbf{y}) = -\frac{D}{8\pi}\left[2(1+\nu)(1+\log r) + (1-\nu)\cos 2\beta\right] \tag{8}$$

$$K_n^*(\mathbf{x},\mathbf{y}) = -\frac{D}{4\pi r}[2 + (1-\nu)\cos 2\beta]\cos\beta + \frac{1-\nu}{4\pi\rho}D\cos 2\beta \tag{9}$$

where $\cos\beta = r_{,k}(\mathbf{y})n_k(\mathbf{y})$, with β being the angle between direction r and n (Fig. 1), and $1/\rho$ is the curvature of the boundary curve S at point $\mathbf{y}$.

Stern [1] derived the complete forms of the direct BIEs based on the Kirchhoff thin plate theory. These BIEs for a plate with a smooth boundary are:

$$\int_S [w^*K_n - K_n^*w + M_n^*\theta - \theta^*M_n]dS(\mathbf{y}) + \int_V w^*qdV(\mathbf{y})$$
$$= \begin{cases} w(\mathbf{x}), & \mathbf{x}\in V; \\ \frac{1}{2}w(\mathbf{x}), & \mathbf{x}\in S(smooth); \\ 0, & \mathbf{x}\notin V\cup S \end{cases} \tag{10}$$

and

$$\int_S \left[w^*_{,\xi}K_n - K_{n,\xi}^*w + M_{n,\xi}^*\theta - \theta_{,\xi}^*M_n\right]dS(\mathbf{y}) + \int_V w^*_{,\xi}qdV(\mathbf{y})$$
$$= \begin{cases} w_{,\xi}(\mathbf{x}), & \mathbf{x}\in V; \\ \frac{1}{2}w_{,\xi}(\mathbf{x}), & \mathbf{x}\in S \text{ (smooth)}; \\ 0, & \mathbf{x}\notin V\cup S \end{cases} \tag{11}$$

in which $\theta = \theta(\mathbf{y}) = \partial w/\partial n$, $M_n = M_n(\mathbf{y})$, and $K_n = K_n(\mathbf{y})$ are the rotation, bending moment, and Kirchhoff equivalent shear force, respectively, ξ is a direction vector associated with the source point $\mathbf{x}$ (Fig. 1). On boundary S, we have $\xi = n(\mathbf{x})$ and $w_{,\xi}(\mathbf{x}) = \theta(\mathbf{x})$. In this work, we ignore the jump terms at the corners if they exist, since the constant elements will be used in the discretization where all the collocation points are away from the corners. In practice, all plates with corners can be considered being rounded off with little effects on the solutions.

When $\mathbf{x} \in S$, we can employ (10) and (11) to solve the unknown boundary variables under given BCs. We usually call (10) with $\mathbf{x} \in S$ as conventional BIE (CBIE) or regular/ordinary BIE, and (11) as hypersingular BIE (HBIE). Once all the boundary variables are known, (10) and (11) with $\mathbf{x} \in V$ (also called representation integrals) can be applied to evaluate the deflection and its derivatives inside the plate.

2.2. Treatment of domain integrals

The domain integral is not easy to be evaluated efficiently if the external load q is complicated. The easiest way is to discretize the domain directly and use numerical integration such as Gauss quadrature to carry out the integration. However, it is too expensive for most cases and sometimes is difficult to implement especially for the perforated plate cases. Aliabadi discussed some methods to deal with domain integrals in [11]. Gao [22] developed a new method for converting domain integrals to boundary integrals. Dual reciprocity method is another efficient method which uses some radial based functions to represent the body force and convert domain integrals to boundary integrals [23]. In this work, we are interested in the behaviors of thin plates under concentrated load and uniformly distributed load so that q is a constant at most and the domain integral can be converted to the boundary integral which is much easier to evaluate. For uniform distributed load q, the formulas for converting boundary integrals are:

$$\int_V qw^*dV(\mathbf{y}) = q\int_S \tilde{w}^* \, dS(\mathbf{y}) \qquad \int_V qw^*_{,\varsigma}dV(\mathbf{y}) = q\int_S \tilde{w}^*_{,\varsigma}dS(\mathbf{y}) \qquad (12)$$

where

$$\tilde{w}^*(\mathbf{x},\mathbf{y}) = \frac{1}{8\pi}\frac{r^3}{16}(4\log r - 1)\cos\beta$$
$$\tilde{w}^*_{,\varsigma}(\mathbf{x},\mathbf{y}) = -\frac{1}{8\pi}\left((\vec{r}\cdot\vec{n})(\vec{r}\cdot\vec{\xi})\log r - \frac{r^2}{4}(2\log r - 1)(\vec{n}\cdot\vec{\xi})\right) \qquad (13)$$

If $q(\mathbf{y}) = P\delta(\tilde{\mathbf{x}},\mathbf{y})$ where P is a concentrated load, the domain integral can be simplified as:

$$\int_V qw^*dV(\mathbf{y}) = Pw^*(\mathbf{x},\tilde{\mathbf{x}})$$

with $\tilde{\mathbf{x}}$ being the point where P is applied. Once this conversion is done, Eqs. (10) and (11) involve only boundary variables. Therefore, only the boundary need to be discretized in order to find the solution of the unknown variables on the boundary.

3. Fast multipole formulations

The main idea of the FMM is to implement the matrix-vector multiplication without forming the entire matrix explicitly and to use an iterative solver to obtain the solution. In the FMM, all elements are usually divided into two parts: the elements close to the source point and the elements far away from the source point. The interactions between the first part of elements and source points are still evaluated by direct integration as in the conventional BEM. For the second part of elements, fast multipole expansions will be used. In this section, the complex notation of the kernel functions, expansions and translations in the FMM are derived for the BIEs for the thin plate bending problem.

3.1. Complex Representations of the Kernels

We utilize some formulations of the fast multipole method for 2-D potential problems to derive the complex notation of kernel functions for thin plate bending problems. In 2-D potential problems [18], the complex notation of kernel functions is usually used such that it is easier to find the related expansions and translations.

Define the complex number z_0 and z as: $z_0 = x_1 + ix_2$ and $z = y_1 + iy_2$ where x_1 and x_2 are the ordinates of $\mathbf{x}$, and y_1 and y_2 are the ordinates of $\mathbf{y}$. The complex notation for kernel $w^*(\mathbf{x},\mathbf{y})$ is found to be:

$$w^*(z_0,z) = -\frac{1}{4}(z_0-z)\overline{(z_0-z)}G(z_0,z) \qquad (14)$$

where the over bar indicates complex conjugate and G is the Green's function (in complex form) for 2-D potential problems which is given by [18]:

$$G(z_0,z) = -\frac{1}{2\pi}\log(z_0-z)$$

In the following, z and $\bar{z}$ are considered as two independent variables and $(\ )' = \partial(\ )/\partial z_0$.

It is not straightforward to derive the complex forms of kernels directly. To facilitate the derivations, the following auxiliary expressions are derived firstly (see Appendix):

$$\frac{\cos\beta}{r} = \frac{\vec{r}\cdot\vec{n}}{r^2} = Re\left\{\frac{\overline{n(z)}}{\overline{z-z_0}}\right\} = Re\left\{2\pi\overline{n(z)G'(z_0,z)}\right\}$$

$$\frac{\cos\beta_0}{r} = -\frac{\vec{r}\cdot\vec{\xi}}{r^2} = -Re\left\{\frac{\overline{\xi(z_0)}}{\overline{z-z_0}}\right\} = -Re\left\{2\pi\overline{\xi(z_0)G'(z_0,z)}\right\}$$

$$\cos\varphi_0 = \vec{n}\cdot\vec{\xi} = Re\left\{n(z)\cdot\overline{\xi(z_0)}\right\}$$

$$\frac{(2\cos\beta\cos\beta_0 + \cos\varphi_0)}{r^2} = -Re\left\{\frac{\overline{n(z)\xi(z_0)}}{(\overline{z-z_0})^2}\right\}$$

$$= -Re\left\{2\pi\overline{\xi(z_0)n(z)G''(z_0,z)}\right\}$$

$$\cos 2\beta = Re\left\{\frac{z-z_0}{\overline{z-z_0}}\overline{n^2(z)}\right\} = Re\left\{2\pi(z-z_0)\overline{n^2(z)G'(z_0,z)}\right\} \qquad (15)$$

where $n(z)$ is the unit outward normal vector at point z and $n(z) = n_1 + in_2$, and β_0 is the angle between directions $\vec{r}$ and $\vec{\xi}$ (Fig. 1).

Substituting them into the real forms of the kernel functions, the corresponding complex forms of kernel functions are obtained immediately. The complex forms of the other three kernel functions for the CBIE are:

$$\theta^*(z_0,z) = (z-z_0)\left(-\frac{1}{4}(G(z_0,z) + \overline{G(z_0,z)}) + \frac{1}{8\pi}\right)\overline{n(z)} \qquad (16)$$

$$M_n^*(z_0,z) = -D\left(\frac{(1-v)}{4}(z-z_0)\overline{G'(z_0,z)n^2(z)}\right.$$
$$\left. + \left(-\frac{1}{4}\left(G(z_0,z) + \overline{G(z_0,z)}\right) + \frac{1}{4\pi}\right)(1+v)\right) \qquad (17)$$

$$K_n^*(z_0,z) = -\frac{D}{2}\left(\frac{1}{2}(1-v)((z-z_0)\overline{G''(z_0,z)n^3(z)} + \overline{n(z)G'(z_0,z)})\right.$$
$$\left. + 2\overline{G'(z_0,z)n(z)} - \frac{1-v}{\rho}(z-z_0)\overline{G'(z_0,z)n^2(z)}\right) \qquad (18)$$

The complex representations of the kernel functions for the HBIE are:

$$w^*_{,\xi}(z_0,z) = -(z-z_0)\left(-\frac{1}{4}(G(z_0,z) + \overline{G(z_0,z)}) + \frac{1}{8\pi}\right)\overline{\xi(z_0)} \qquad (19)$$

$$\theta^*_{,\xi}(z_0,z) = -\frac{1}{4}\overline{G'(z_0,z)}(z-z_0)\overline{n(z)\xi(z_0)}$$
$$- \left(-\frac{1}{4}(G(z_0,z) + \overline{G(z_0,z)}) + \frac{1}{4\pi}\right)n(z)\overline{\xi(z_0)} \qquad (20)$$

$$M^*_{n,\xi}(z_0,z) = \frac{D(1-v)}{4}((z_0-z)\overline{G''(z_0,z)n^2(z)\xi(z_0)} + n^2(z)\overline{\xi(z_0)}G')$$

$$+\frac{D(1+v)}{2}\overline{G'(z_0,z)\xi(z_0)} \tag{21}$$

$$K^*_{n,\xi}(z_0,z)=\frac{D}{4}\Big((1-v)\big(-(z-z_0)\overline{n^3(z)\xi(z_0)G'''(z_0,z)}-\overline{n(z)\xi(z_0)G''(z_0,z)}$$
$$+n^3(z)\overline{\xi(z_0)}G''(z_0,z)-4\overline{n(z)\xi(z_0)G''(z_0,z)}\big)$$
$$+\frac{D(1-v)}{2\rho}\cdot\Big((z-z_0)\overline{n^2(z)\xi(z_0)G''(z_0,z)}-n^2(z)\overline{\xi(z_0)}G'(z_0,z)\Big) \tag{22}$$

where $\xi(z_0)$ is the unit normal vector at point z_0 and $\xi(z_0)=\xi_1+i\xi_2$.

Substituting (15) into (13), we obtain the complex representations for $\tilde{w}^*$ and $\tilde{w}^*_{,\xi}$:

$$\tilde{w}^*(z_0,z)=-\frac{1}{32}(z_0-z)(\overline{z_0-z})((z_0-z)\overline{n(z)}$$
$$+(\overline{z_0-z})n(z))\Big(G(z_0,z)+\frac{1}{8\pi}\Big)$$

$$\tilde{w}^*_{,\xi}(z_0,z)=\frac{1}{16}(z-z_0)^2\overline{\xi(z)n(z)}(G(z_0,z)$$
$$+\overline{G(z_0,z)})-\frac{1}{32\pi}(z-z_0)(\overline{z-z_0})\overline{\xi(z_0)}n(z) \tag{23}$$

If q represents a concentrated load, it is not necessary to use the FMM because the order of operations in evaluating the domain integrals is already $O(N)$.

3.2. Multipole expansions and moment to moment translations

Let z_c be a multipole expansion point close to z (Fig. 2) and apply Taylor series expansion. The multipole expansion of $G(z_0,z)$ and its derivatives are [18]:

$$G(z_0,z)=-\frac{1}{2\pi}\log(z_0-z)=\frac{1}{2\pi}\sum_{k=0}^{\infty}O_k(z_0-z_c)I_k(z-z_c)$$
$$\frac{\partial^{(l)}G(z_0,z)}{\partial z_0^{(l)}}=(-1)^l\frac{1}{2\pi}\sum_{k=0}^{\infty}O_{k+l}(z_0-z_c)I_k(z-z_c)\quad\text{for}\quad l=1,2,\ldots, \tag{24}$$

where the two auxiliary functions are defined as [18]:

$$I_k(z)=\frac{z^k}{k!}\ \text{for}\ k\geq0$$

$$O_0(z)=-\log(z)\ \text{and}\ O_k(z)=\frac{(k-1)!}{z^k}\ \text{for}\ k\geq1$$

Substituting (24) into (19)–(22) directly gives us the multipole expansion of the CBIE:

$$\int_S[w^*(z_0,z)K_n-K^*_n(z_0,z)w+M^*_n(z_0,z)\theta-\theta^*(z_0,z)M_n]dS(z)$$
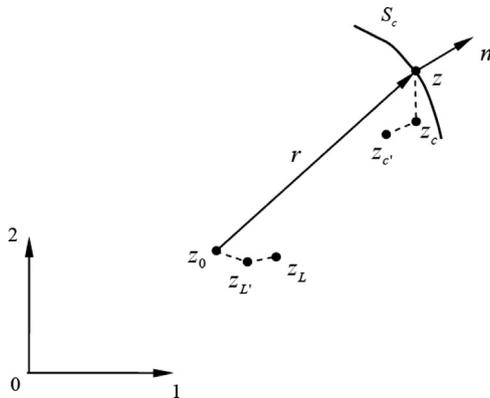$$=\frac{1}{8\pi}\Big[\sum_{k=0}^{\infty}O_k(z_0-z_c)N_k(z_c)+z_0\sum_{k=0}^{\infty}O_k(z_0-z_c)\tilde{N}_k(z_c)$$

Fig. 2. Complex notation and the related points for fast multipole expansions.

$$-|z_0|^2\sum_{k=0}^{\infty}O_k(z_0-z_c)P_k(z_c)+\sum_{k=0}^{\infty}\overline{O_k(z_0-z_c)}R_k(z_c)$$
$$+z_0\sum_{k=0}^{\infty}\overline{O_k(z_0-z_c)}\tilde{R}_k(z_c)+S_1+z_0S_2\Big] \tag{25}$$

where

$$N_k(z_c)=\int_S I_k(z-z_c)(z\overline{n(z)}M_n-|z|^2K_n)dS(z),\ \text{for}\ k\geq0 \tag{26}$$

$$\tilde{N}_k(z_c)=\int_S I_k(z-z_c)(\overline{z}K_n-\overline{n(z)}M_n)dS(z),\ \text{for}\ k\geq0 \tag{27}$$

$$P_k(z_c)=\int_S I_k(z-z_c)K_ndS(z),\ \text{for}\ k\geq0 \tag{28}$$

$$R_0(z_c)=\int_S(z\overline{n(z)}M_n(z)+2D(1+v)\theta(z))dS(z)$$

$$R_1(z_c)=\int_S\overline{(z-z_c)}(z\overline{n(z)}M_n(z)+2D(1+v)\theta(z))dS(z)$$
$$+\int_S\Big(D(1-v)z\overline{n^2(z)}\Big(\theta(z)+\frac{2}{\rho}w(z)\Big)-(5-v)D\overline{n(z)}w\Big)dS(z)$$

$$R_k(z_c)=\int_S\overline{I_k(z-z_c)}(z\overline{n(z)}M_n(z)+2D(1+v)\theta(z))dS(z)$$
$$+\int_S\overline{I_{k-1}(z-z_c)}\Big(D(1-v)z\overline{n^2(z)}\Big(\theta(z)+\frac{2}{\rho}w(z)\Big)-(5-v)D\overline{n(z)}w\Big)dS(z)$$
$$+\int_S\overline{I_{k-2}(z-z_c)}D(1-v)z\overline{n^3(z)}w(z)dS(z),\quad\text{for}\ k\geq2 \tag{29}$$

$$\tilde{R}_0(z_c)=\int_S(\overline{z}K_n(z)-\overline{n(z)}M_n(z))dS(z)$$

$$\tilde{R}_1(z_c)=\int_S\overline{(z-z_c)}(\overline{z}K_n(z)-\overline{n(z)}M_n(z))dS(z)$$
$$-\int_S\overline{n^2(z)}D(1-v)\Big(\frac{2}{\rho}w(z)+\theta(z)\Big)dS(z)$$

$$\tilde{R}_k(z_c)=\int_S\overline{I_k(z-z_c)}(\overline{z}K_n(z)-\overline{n(z)}M_n(z))dS(z)$$
$$-\int_S\overline{I_{k-1}(z-z_c)}\overline{n^2(z)}D(1-v)\Big(\frac{2}{\rho}w(z)+\theta(z)\Big)dS(z)$$
$$-\int_S\overline{I_{k-2}(z-z_c)}\overline{n^3(z)}D(1-v)w(z)dS(z),\quad\text{for}\ k\geq2 \tag{30}$$

and the two remaining terms:

$$S_1=-2D(1+v)\int_S\theta(z)dS(z)-\int_S z\overline{n(z)}M_n(z)dS(z)\ \ (=-R_0)$$
$$S_2=\int_S\overline{n(z)}M_n(z)dS(z) \tag{31}$$

Results in (26)–(30) are the moments about z_c for the integrals in the CBIE. Likewise, the multipole expansion for the HBIE is:

$$\int_S[w^*_{,\xi}(z_0,z)K_n-K^*_{n,\xi}(z_0,z)w+M^*_{n,\xi}(z_0,z)\theta-\theta^*_{,\xi}(z_0,z)M_n]dS(z)$$
$$=\frac{1}{8\pi}\overline{\xi(z_0)}\Big[\sum_{k=0}^{\infty}\overline{O_k(z_0-z_c)}\tilde{N}_k(z_c)-z_0\sum_{k=0}^{\infty}O_k(z_0-z_c)P_k(z_c)$$
$$-z_0\sum_{k=0}^{\infty}\overline{O_k(z_0-z_c)}P_k(z_c)$$
$$-\sum_{k=0}^{\infty}\overline{O_{k+1}(z_0-z_c)}R_k(z_c)+\sum_{k=0}^{\infty}O_k(z_0-z_c)\overline{\tilde{R}_k(z_c)}$$
$$+\sum_{k=0}^{\infty}\overline{O_{k+1}(z_0-z_c)}T_k(z_c)+S_3+z_0S_4\Big] \tag{32}$$

where the moments $\tilde{N}_k(z_c)$, $P_k(z_c)$, $R_k(z_c)$ and $\tilde{R}_k(z_c)$ are the same as given in Eqs. (27)–(30), respectively. The new moment $T_k(z_c)$ is given by:

$$T_0(z_c)=\int_S\overline{n(z)}M_n(z)dS(z)\ (=S_2)$$

$$T_1(z_c) = \int_S \overline{(z-z_c)\,n(z)} M_n(z) dS(z)$$

$$+ \int_S \overline{n^2(z)} D(1-v) \left(\frac{2}{\rho} w(z) + \theta(z) \right) dS(z)$$

$$T_k(z_c) = \int_S \overline{I_k(z-z_c)\,n(z)} M_n(z) dS(z)$$

$$+ \int_S \overline{I_{k-1}(z-z_c)}\,\overline{n^2(z)} D(1-v) \left(\frac{2}{\rho} w(z) + \theta(z) \right) dS(z)$$

$$+ \int_S \overline{I_{k-2}(z-z_c)}\,\overline{n^3(z)} D(1-v) w(z) dS(z), \quad \text{for } k \geq 2 \tag{33}$$

and the two remaining terms are:

$$S_3 = 2 \int_S n(z) M_n dS(z) - \int_S z K_n dS(z)$$

$$S_4 = \int_S K_n dS(z) \ (= P_0) \tag{34}$$

If the multipole expansion point z_c is moved to a new location $z_{c'}$ (see Fig. 2), we have the following moment to moment (M2M) translations:

$$N_k(z_{c'}) = \sum_{l=0}^{k} I_{k-l}(z_c - z_{c'}) N_k(z_c)$$

$$\tilde{N}_k(z_{c'}) = \sum_{l=0}^{k} I_{k-l}(z_c - z_{c'}) \tilde{N}_k(z_c)$$

$$P_k(z_{c'}) = \sum_{l=0}^{k} I_{k-l}(z_c - z_{c'}) P_k(z_c)$$

$$R_k(z_{c'}) = \sum_{l=0}^{k} \overline{I_{k-l}(z_c - z_{c'})} R_k(z_c)$$

$$\tilde{R}_k(z_{c'}) = \sum_{l=0}^{k} \overline{I_{k-l}(z_c - z_{c'})} \tilde{R}_k(z_c)$$

$$T_k(z_{c'}) = \sum_{l=0}^{k} \overline{I_{k-l}(z_c - z_{c'})} T_k(z_c) \tag{35}$$

All the M2M translations are exactly the same as used in the 2-D potential case [18].

3.3. Local expansions and translations

Let z_L be a local expansion point close to the source point z_0 (Fig. 2). By using Taylor series expansion, we have the following local expansions for the CBIE:

$$\int_S [w^*(z_0,z)K_n - K_n^*(z_0,z)w + M_n^*(z_0,z)\theta - \theta^*(z_0,z)M_n] dS(z)$$

$$= \frac{1}{8\pi} \left[\sum_{l=0}^{\infty} L_l(z_L) \overline{I_l(z_0 - z_L)} + z_0 \sum_{l=0}^{\infty} \tilde{L}_l(z_L) \overline{I_l(z_0 - z_L)} + \sum_{l=0}^{\infty} U_l(z_L) I_l(z_0 - z_L) \right.$$

$$\left. + z_0 \sum_{l=0}^{\infty} \tilde{U}_l(z_l) I_l(z_0 - z_L) - |z_0|^2 \sum_{l=0}^{\infty} V_l(z_l) I_l(z_0 - z_L) + S_1 + z_0 S_2 \right] \tag{36}$$

and for the HBIE:

$$\int_S [w_{,\xi}^*(z_0,z)K_n - K_{n,\xi}^*(z_0,z)w + M_{n,\xi}^*(z_0,z)\theta - \theta_{,\xi}^*(z_0,z)M_n] dS(z)$$

$$= \frac{1}{8\pi} \overline{\xi(z_0)} \left[\sum_{l=1}^{\infty} L_l(z_L) \overline{I_{l-1}(z_0 - z_L)} + \sum_{l=0}^{\infty} \overline{\tilde{L}_l(z_L)} I_l(z_0 - z_L) \right.$$

$$+ \sum_{l=0}^{\infty} \overline{\tilde{U}_l(z_L)} I_l(z_0 - z_L) - z_0 \sum_{l=0}^{\infty} V_l(z_L) I_l(z_0 - z_L) - z_0 \sum_{l=0}^{\infty} \overline{V_l(z_L) I_l(z_0 - z_L)}$$

$$\left. - \sum_{l=1}^{\infty} W_l(z_L) \overline{I_{l-1}(z_0 - z_L)} + S_3 + z_0 S_4 \right] \tag{37}$$

where the expansion coefficients are given by the following moment to local (M2L) translation:

$$L_l(z_L) = (-1)^l \sum_{k=0}^{\infty} \overline{O_{k+l}(z_L - z_c)} R_k(z_c)$$

$$\tilde{L}_l(z_L) = (-1)^l \sum_{k=0}^{\infty} \overline{O_{k+l}(z_L - z_c)} \tilde{R}_k(z_c)$$

$$U_l(z_L) = (-1)^l \sum_{k=0}^{\infty} O_{k+l}(z_L - z_c) N_k(z_c)$$

$$\tilde{U}_l(z_L) = (-1)^l \sum_{k=0}^{\infty} O_{k+l}(z_L - z_c) \tilde{N}_k(z_c)$$

$$V_l(z_L) = (-1)^l \sum_{k=0}^{\infty} O_{k+l}(z_L - z_c) P_k(z_c)$$

$$W_l(z_L) = (-1)^l \sum_{k=0}^{\infty} \overline{O_{k+l}(z_L - z_c)} T_k(z_c) \tag{38}$$

for $l \geq 0$.

If the local expansion point is moved from z_L to $z_{L'}$ (Fig. 2), the new local expansion coefficients are given by the following local to local (L2L) translations:

$$L_l(z_{L'}) = \sum_{m=l}^{\infty} \overline{I_{m-l}(z_{L'} - z_L)} L_m(z_L)$$

$$\tilde{L}_l(z_{L'}) = \sum_{m=l}^{\infty} \overline{I_{m-l}(z_{L'} - z_L)} \tilde{L}_m(z_L)$$

$$U_l(z_{L'}) = \sum_{m=l}^{\infty} I_{m-l}(z_{L'} - z_L) U_m(z_L)$$

$$\tilde{U}_l(z_{L'}) = \sum_{m=l}^{\infty} I_{m-l}(z_{L'} - z_L) \tilde{U}_m(z_L)$$

$$V_l(z_{L'}) = \sum_{m=l}^{\infty} I_{m-l}(z_{L'} - z_L) V_m(z_L)$$

$$W_l(z_{L'}) = \sum_{m=l}^{\infty} \overline{I_{m-l}(z_{L'} - z_L)} W_m(z_L) \tag{39}$$

for $l \geq 0$. Note that all the translation coefficients (M2M, M2L and L2L) are the same as for the 2-D potential case [18]. Therefore, no extra effort is needed in implementation of these translations based on the 2-D potential code [18].

3.4. Expansions and translations of the domain related integrals

The expansions and translations of the domain related integrals are derived for uniform distributed load q. For the first integral in (12) for the CBIE, the multipole expansion is:

$$q \int_S \tilde{w}^*(z_0,z) dS(\mathbf{y})$$

$$= -\frac{q}{64\pi} \left[\sum_{k=0}^{\infty} O_k(z_0-z_c) R_k^1(z_c) - z_0 \sum_{k=0}^{\infty} O_k(z_0-z_c) R_k^2(z_c) \right.$$

$$+ |z_0|^2 \sum_{k=0}^{\infty} O_k(z_0-z_c) R_k^3(z_c) + z_0^2 \sum_{k=0}^{\infty} O_k(z_0-z_c) R_k^4(z_c)$$

$$- z_0 |z_0|^2 \sum_{k=0}^{\infty} O_k(z_0-z_c) R_k^5(z_c) - z_0 \sum_{k=0}^{\infty} \overline{O_k(z_0-z_c)} R_k^8(z_c)$$

$$\left. + z_0^2 \sum_{k=0}^{\infty} \overline{O_k(z_0-z_c)} R_k^9(z_c) - z_0 |z_0|^2 \sum_{k=0}^{\infty} \overline{O_k(z_0-z_c)} R_k^{10}(z_c) \right]$$

$$- \frac{q}{128\pi} (S_5 + z_0 S_6 + + |z_0|^2 S_7 + z_0^2 S_8 + z_0 |z_0|^2 S_9) \tag{40}$$

and for the second integral in (12) for the HBIE, the multipole expansion is:

$$q \int_S \tilde{w}_{,\xi}^* dS(\mathbf{y})$$

$$= \frac{q}{32\pi} \overline{\xi(z_0)} \left[z_0^2 \sum_{k=0}^{\infty} O_k(z_0-z_c) R_k^5(z_c) + \sum_{k=0}^{\infty} O_k(z_0-z_c) R_k^6(z_c) \right.$$

$$- z_0 \sum_{k=0}^{\infty} O_k(z_0-z_c) R_k^7(z_c) + z_0^2 \sum_{k=0}^{\infty} \overline{O_k(z_0-z_c)} R_k^{10}(z_c)$$

$$+ \sum_{k=0}^{\infty} \overline{O_k(z_0-z_c)} R_k^{11}(z_c)$$

$$-z_0 \sum_{k=0}^{\infty} \overline{O_k(z_0-z_c)} R_k^{12}(z_c)\Bigg] - \frac{q}{32\pi} \overline{\xi(z_c)}(S_{10} + z_0 S_{11} - \overline{z_0 S_8} - \left|z_0\right|^2 \overline{S_9})$$

$$(41)$$

where

$$R_k^1(z_c) = \int_S I_k(z-z_c)\left|z\right|^2 (z\overline{n(z)} + \overline{z}n(z))dS(z)$$

$$R_k^2(z_c) = \int_S I_k(z-z_c)(2\left|z\right|^2 \overline{n(z)} + \overline{z}^2 n(z))dS(z)$$

$$R_k^3(z_c) = \int_S I_k(z-z_c)(2z\overline{n(z)} + 2\overline{z}n(z))dS(z)$$

$$R_k^4(z_c) = \int_S I_k(z-z_c)\overline{z n(z)}dS(z)$$

$$R_k^5(z_c) = \int_S I_k(z-z_c)\overline{n(z)}dS(z)$$

$$R_k^6(z_c) = \int_S I_k(z-z_c)z^2 \overline{n(z)}dS(z)$$

$$R_k^7(z_c) = 2\int_S I_k(z-z_c)z\overline{n(z)}dS(z)$$

$$R_k^8(z_c) = \int_S \overline{I_k(z-z_c)}[2\left|z\right|^2 \overline{n(z)} + \overline{z}^2 n(z)]dS(z)$$

$$R_k^9(z_c) = \int_S \overline{I_k(z-z_c)z n(z)}dS(z)$$

$$R_k^{10}(z_c) = \int_S \overline{I_k(z-z_c)n(z)}dS(z)$$

$$R_k^{11}(z_c) = \int_S \overline{I_k(z-z_c)z^2 n(z)}dS(z)$$

$$R_k^{12}(z_c) = 2\int_S \overline{I_k(z-z_c)z n(z)}dS(z) \qquad (42)$$

and

$$S_5 = \int_S z\left|z\right|^2 \overline{n(z)}dS(z), \quad S_6 = -\int_S \left[2\left|z\right|^2 \overline{n(z)} + \overline{z}^2 n(z)\right]dS(z),$$

$$S_7 = 2\int_S z\overline{n(z)}dS(z), \quad S_8 = \int_S \overline{z n(z)}dS(z),$$

$$S_9 = -\int_S \overline{n(z)}dS(z), \quad S_{10} = \int_S \left|z\right|^2 n(z)dS(z),$$

$$S_{11} = -\int_S \overline{z}n(z)dS(z) \qquad (43)$$

The subscript k in Eq. (42) means k-th moment and the superscripts represent different moments. That is, we have 12 different moments in total for the two domain related integrals. The M2M translations for above moments are operated similarly as the ones in the previous section. The local expansions for two domain related integrals in the CBIE and HBIE are:

$$q\int_S \tilde{w}^*(z_0,z)dS(\mathbf{y})$$

$$= -\frac{q}{64\pi}\Bigg[\sum_{l=0}^{\infty} L_l^1(z_L)I_l(z_0-z_L) - z_0 \sum_{l=0}^{\infty} L_l^2(z_L)I_l(z_0-z_L)$$

$$+ \left|z_0\right|^2 \sum_{l=0}^{\infty} L_l^3(z_L)I_l(z_0-z_L) + z_0^2 \sum_{l=0}^{\infty} L_l^4(z_L)I_l(z_0-z_L)$$

$$- z_0\left|z_0\right|^2 \sum_{l=0}^{\infty} L_l^5(z_L)I_l(z_0-z_L) - z_0 \sum_{l=0}^{\infty} L_l^8(z_L)\overline{I_l(z_0-z_L)}$$

$$+ z_0^2 \sum_{l=0}^{\infty} L_l^9(z_L)\overline{I_l(z_0-z_L)} - z_0\left|z_0\right|^2 \sum_{l=0}^{\infty} L_l^{10}(z_L)\overline{I_l(z_0-z_L)}\Bigg]$$

$$- \frac{q}{128\pi}(S_5 + z_0 S_6 + + \left|z_0\right|^2 S_7 + z_0^2 S_8 + z_0\left|z_0\right|^2 S_9) \qquad (44)$$

and

$$q\int_S \tilde{w}_{,\xi}^* dS(\mathbf{y})$$

$$= \frac{q}{32\pi}\overline{\xi(z_0)}\Bigg[z_0^2 \sum_{l=0}^{\infty} L_l^5(z_L)I_l(z_0-z_L) + \sum_{l=0}^{\infty} L_l^6(z_L)I_l(z_0-z_L)$$

$$- z_0 \sum_{l=0}^{\infty} L_l^7(z_L)I_l(z_0-z_L) + z_0^2 \sum_{l=0}^{\infty} L_l^{10}(z_L)\overline{I_l(z_0-z_L)}$$

$$+ \sum_{l=0}^{\infty} L_l^{11}(z_L)\overline{I_l(z_0-z_L)} - z_0 \sum_{l=0}^{\infty} L_l^{12}(z_L)\overline{I_l(z_0-z_L)}\Bigg]$$

$$- \frac{q}{32\pi}\overline{\xi(z_0)}(S_{10} + z_0 S_{11} - \overline{z_0 S_8} - \left|z_0\right|^2 \overline{S_9}) \qquad (45)$$

The coefficients are given by the M2L translations which are the same as the ones in the previous section:

$$L_l^i(z_L) = (-1)^l \sum_{k=0}^{\infty} O_{k+l}(z_L-z_c)R_k^i(z_c), \quad \text{for } i=1,2,\cdots,7; \qquad (46)$$

$$L_l^i(z_L) = (-1)^l \sum_{k=0}^{\infty} \overline{O_{k+l}(z_L-z_c)}R_k^i(z_c), \quad \text{for } i=8,9,\cdots,12 \qquad (47)$$

The L2L translations for these local expansion coefficients are also similar to the ones in the previous section:

$$L_l^i(z_{L'}) = \sum_{m=l}^{\infty} I_{m-l}(z_{L'}-z_L)L_m^i(z_L), \quad \text{for } i=1,2,\cdots,7; \qquad (48)$$

$$L_l^i(z_{L'}) = \sum_{m=l}^{\infty} \overline{I_{m-l}(z_{L'}-z_L)}L_m^i(z_L), \quad \text{for } i=8,9,\cdots,12 \qquad (49)$$

Table 1
Maximum deflections of the plates under uniform distributed load and concentrated load.

Loading	Type of Plate	No. of elements	Fast multipole BEM α	Conventional BEM α	Exact solution [25] ($\alpha Pa^2/D$ or $\alpha qa^4/D$) α
Uniform distributed load q	Square plate	40	0.004064	0.004064	0.004062
		80	0.004062	0.004061	
		160	0.004061	0.004062	
	Circle plate	128	0.0632	0.0632	0.0637
		252	0.0635	0.0635	
		504	0.0636	0.0636	
Concentrated load P	Square plate	40	0.01160	0.01160	0.01160
		80	0.01160	0.01160	
		160	0.01160	0.01160	
	Circle plate	128	0.0502	0.0502	0.0505
		252	0.0504	0.0503	
		504	0.0504	0.0504	

4. Numerical examples

Several benchmark plate bending problems are studied first to show the accuracy and efficiency of the developed fast multipole BEM for solving thin plate bending problems. Then more complicated cases of perforated plate models with about 500,000 DOFs are solved. In all the numerical examples, Young's modulus $E = 70$ GPa, Poisson's ratio $v = 0.3$, thickness of the plate $h = 0.05$m, the uniformly distributed load $q = 0.1$MPa, and the concentrated load $P = 10$KN. Constant line elements are used in the BEM, where all the singular and hypersingular integrals are calculated analytically based on the definitions of the CPV and HFP integrals, respectively (see, e.g., Ref. [18]).

For the fast multipole BEM, the numbers of terms for both multipole and local expansions are set to 15, and the maximum number of elements in a leaf are set to 20. Other numbers of expansion terms equal to 5 and 10 are also tested, and it is found that results with 5 expansion terms are not accurate, while results with 10 expansion terms are within 1% of those with 15 terms. GMRES [24] iterative solver is used to solve all the linear equations and the tolerance for convergence is set to 10^{-8}. A block diagonal preconditioner is used with the GMRES solver. For the conventional BEM, the LAPACK package is applied to solve the linear system. All the examples are run on a desktop PC with an Intel Core Duo 2 CPU and 8 GB RAM.

4.1. Square and circular plate models

Two cases are presented to verify the fast multipole BEM first. Simply supported square and circular plates without holes under uniformly distributed load and concentrated load applied at the center are given. The exact solutions of maximum deflection w_{max} are given in [25] in terms of non-dimensional coefficients α and β. For the concentrated load: $w_{max} = \alpha P a^2 / D$ and for the uniform distributed load: $w_{max} = \alpha q a^4 / D$ where a is the length of edges of the square plate or the radius of the circular plate.

From Table 1, we can see the maximum deflections solved by the fast multipole BEM agree very well with the results of the conventional BEM, and both the BEM results agree with the exact solutions for all the cases.

4.2. Plates with one hole

Next, we present some examples of plates with one hole under uniformly distributed load to show the capabilities of the developed fast multipole BEM in dealing with multi-connected domain problems and its efficiencies in solutions.

The first example is a circular plate of radius $R = 1$ m with a center hole of radius $r = 0.25$ m (Fig. 3). The outer boundary of the plate is simply supported and the inner boundary (edge of the hole) is free. Under the uniformly distributed load q, the maximum deflection is on the edge of the hole. The fast multipole BEM results are obtained with several meshes and compared with the FEM (ANSYS®) solutions using 4-node shell elements. A comparison of the convergence of the fast multipole BEM and FEM solutions is shown in Fig. 4, and good agreement is observed. Both the fast multipole BEM and FEM solutions converge as the numbers of the elements are sufficiently large.

Next we consider a circular plate with an off-center hole as shown in Fig. 5. The radius of the plate is $R = 1$ m, the radius of the hole is $r = 0.15$ m, and the hole is centered at $x = y = 0.4$ m location. Again the plate is simply supported on the outer boundary and the edge of the hole is free. Fig. 6 shows the computed values of the deflection on the edge of the hole using the fast multipole BEM and compared with those using the FEM. The horizontal axis is the angle (in radian) defined as in the right
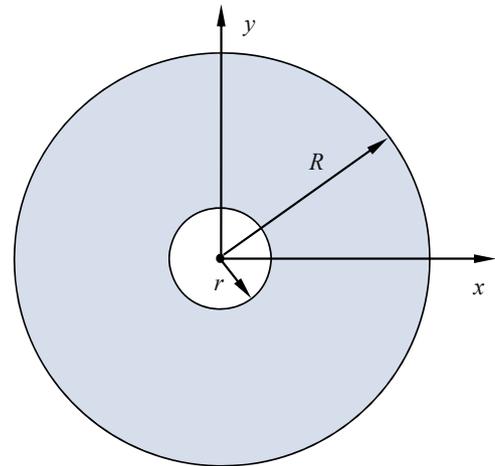

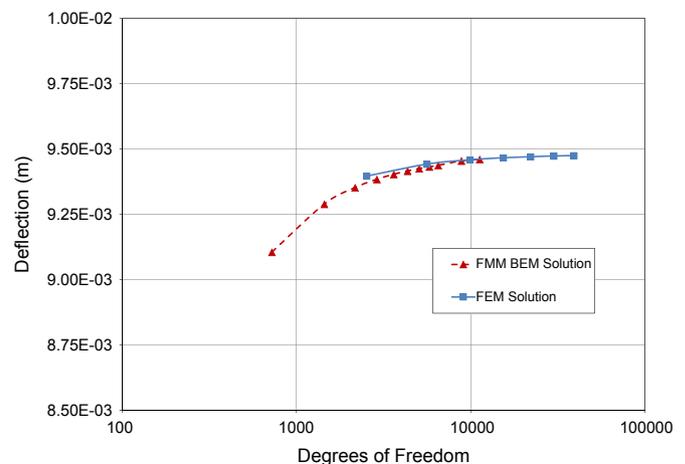**Fig. 3.** A circular plate with a center hole.

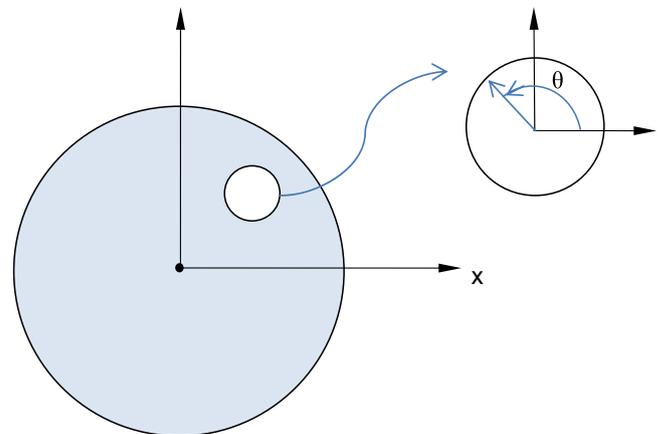**Fig. 4.** Computed maximum deflection for the circular plate with a center hole.

Fig. 5. A circular plate with an off-center hole.

upper corner of Fig. 5 where axis x' and y' are parallel to axis x and y, respectively. A total of 3240 line elements are used in the fast multipole BEM model and a total of 12610 shell elements are used in the FEM model for this comparison. Very good agreement between the fast multipole BEM results and FEM results is achieved as shown in Fig. 6.

The above examples demonstrate the capability for fast multipole BEM to solve multi-connected domain problems and indicate
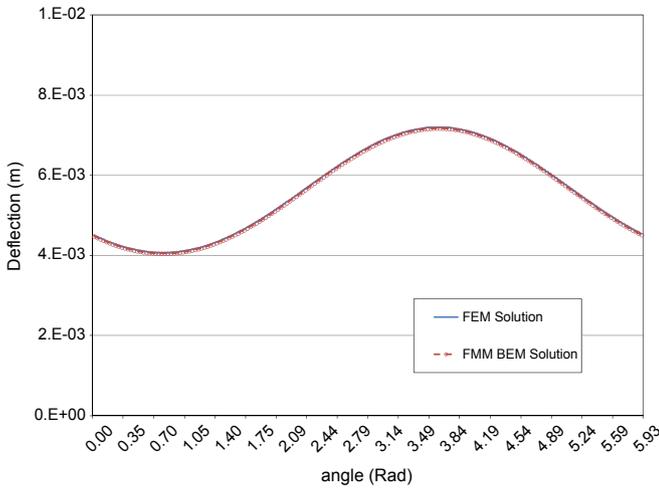
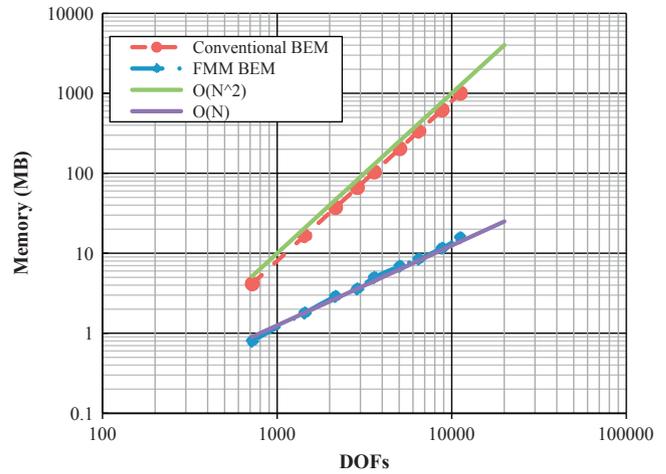**Fig. 6.** Deflection on the edge of the hole for the model in Fig. 5.

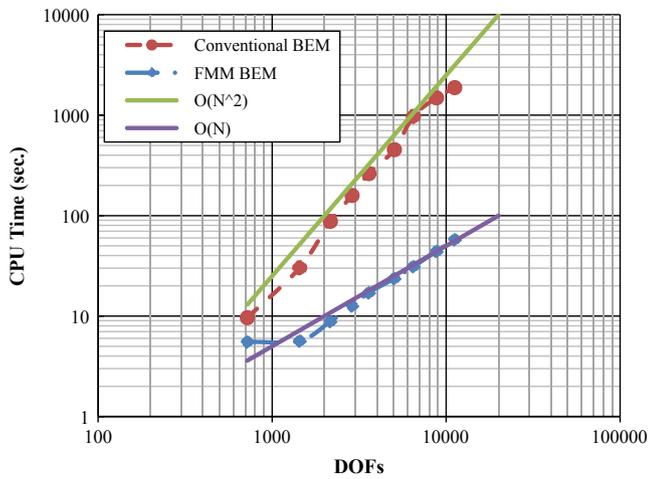**Fig. 8.** Comparison of used memory between FMM BEM and Conventional BEM.

Fig. 7. Comparison of CPU time between FMM BEM and Conventional BEM.

Fig. 9. The BEM models of the perforated plate.

that the complex notation for all the kernels is correct. We now solve the model in Fig. 3 again using both the conventional BEM and fast multipole BEM to show the efficiency of fast multipole BEM without using any pre-conditioner (only in this case).

Figs. 7 and 8 show the CPU time and computer memory used by the conventional BEM and fast multipole BEM. Here the used memory only includes the memory allocated by the program. Clearly, the fast multipole BEM requires much less CPU time and computer memory. As the number of degrees of freedom of the model increases, the fast multipole BEM is even more efficient compared with the conventional BEM, which enables the BEM to be used in solving large-scale plate bending problems. In addition, we can see that the data of the used CPU time and memory are matched very well with the trend lines for both fast multipole BEM and conventional BEM. As it is mentioned before, the conventional BEM requires $O(N^2)$ operations (with iterative solver), while the fast multipole BEM can achieve $O(N)$ efficiency. Figs. 7 and 8 support this conclusion.

4.3. Perforated plate models

We apply the developed fast multipole BEM to solve some perforated plate models. Here we use the BEM to analyze plates with 4, 16, 36 and 64 holes under a concentrated load and evaluate the effective bending rigidity of these perforated plate models.
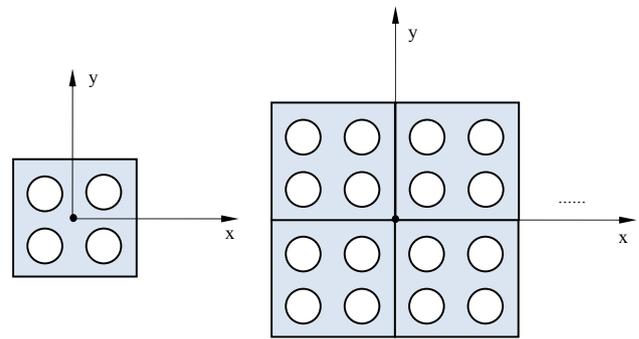
The models of perforated plates are constructed in the following way. We use a square plate with 4 holes as a basic pattern (see the plot on the left-hand side of Fig. 9). The square plate has an edge length of 1 m. The four holes have the same radius of 0.1 m and are centered at $x = y = \pm 0.25$ m. Then we directly add some basic patterns together to construct the larger perforated plate models. Only the boundaries of the new larger models are kept. Any other boundaries of the basic patterns that are inside the larger models are deleted. For example, to construct the model with 16 holes, we just use 4 patterns and add them together as shown on the right-hand side of Fig. 9.

In Table 1, the maximum deflection of simply supported plates subjected to the concentrated load at the center is written as:

$$w_{\max} = \frac{\alpha P a^2}{D} \tag{50}$$

where P represents the concentrated load, a is the length of the edges of the plates, D is the bending rigidity and α is a non-dimensional number. To calculate the effective bending rigidity of the perforated plates, we use a similar formula:

$$w'_{\max} = \frac{\alpha P a^2}{D_{eff}} \tag{51}$$

where α and P are the same values as the cases of simply supported plates without holes under a center concentrated load, $w'_{\max}$ is the maximum deflection of the perforated plate, and D_{eff} is the effective bending rigidity. Dividing (50) by (51), we have:

$$\eta = \frac{D_{eff}}{D} = \frac{w_{\max}}{w'_{\max}} \tag{52}$$

Table 2
Comparison of effective bending rigidity for a perforated plate.

No. of holes	η			
	FMM BEM	Conventional BEM	FEM	Analytical results from [26]
4	0.83424	0.83426	0.83300	0.76
16	0.79357	–	0.78922	
36	0.78785	–	0.77619	
64	0.77442	–	0.77079	

The ratio η of the stiffness is associated with the maximum deflections of the simple plate (without holes) and the perforated plate. Eq. (52) is applied to estimate the effective bending rigidity in this example.

Analytic predictions of the effective rigidity of the perforated plates are available in the literature. Meijers first proposed the analytic results of the effective elastic constants for perforated plates in [26]. He derived formulas for predicting the infinite perforated plates with square patterns and triangular patterns, respectively, by using complex analysis. Later, O'Donnell [27] conducted some experiments and suggested new formulas to predict the effective elastic constants. Lee and Kim [28], also presented a numerical way to estimate the effective elastic constants. In this work, we compare our results with Meijers' analytical results in [26].

In Table 2, we can see that as the number of the holes increase, the ratio η calculated by fast multipole BEM converges to a stable value which agrees well with the analytical solution [26]. Note that Meijers' results are suitable for infinitely large perforated plate models. So as the number of holes in our cases increases, the effective bending rigidity should approach Meijers' result. Table 2 supports this conclusion. We also use the conventional BEM and FEM to solve these problems. The conventional BEM can solve the case of a perforated plate model with only four holes. For the cases with more holes, the desktop PC used does not have enough memory needed for the conventional BEM to run the job.

For the largest model with 64 holes, the BEM model has 492,000 unknowns (246,000 constant elements), while the FEM model has 1,259,142 unknowns (204,800 Q4 elements). However, the FEM model was solved in about 6 minutes (using *ANSYS* with the sparse solver and on multi cores), while the BEM model was solved in hours (on a single core) with the same PC. This is due to the fact that a very small tolerance (10^{-8}) for the GMRES solver was used in the BEM solution, and the fast multipole BEM implementation has not been optimized. Further improvements in the fast multipole BEM formulation and code need to be made.

5. Conclusions

In this paper, a fast multipole BEM for thin plate bending problems is presented for the first time. The complex notation is used and the kernels are expressed in complex variables relating to the kernels for the 2-D potential case, which facilitates straightforward implementations for the multipole and local expansions and related translations. However, the expressions for those expansions are quite lengthy and consume much more computing time than in the case of 2-D potential problems. Further investigation on reducing the complexity of the expansions need to be conducted so that the BEM can be applied to solve practical and large models of perforated plates. With even larger numbers of holes and random distributions of the holes in perforated plate models, the BEM should have advantages over the FEM in both meshing stages and solutions.

The Kirchhoff plate theory is not accurate to describe the behaviors of thick plates under transverse loading. As future work, the fast multipole BEM based on the Reissner–Mindlin theory for solving thick plate bending problems can be developed. The BEM can also be applied to analyze the bending problems of jointed plates or plate assemblies in structures. Another potential area for improvement is the application of other fast BEM approaches such as the adaptive cross approximation method [29,30] for solving plate bending problems, which is easier to implement and can offer additional advantages to the BEM such as in parallel computing.

Appendix

In the appendix, we derive the results in Eq. (15). First, we introduce the following notation. Assume **x** and **y** are two points in the 2-D space, and $r = |\mathbf{y}-\mathbf{x}|$ is the distance between **x** and **y**:

$$r = \sqrt{(y_1-x_1)^2 + (y_2-x_2)^2}$$

where x_1, x_2, y_1 and y_2 are the coordinates of **x** and **y**, respectively. For convenience, we use $dx = y_1-x_1$ and $dy = y_2-x_2$. Now r can be rewritten as:

$$r = \sqrt{(dx)^2 + (dy)^2}$$

All the complex variables are defined in the same way as in Section 3.

First Equation:
The real notation of first equation is:

$$\frac{\cos\beta}{r} = \frac{\vec{r}\cdot\vec{n}}{r^2} = \frac{dx\cdot n_1 + dy\cdot n_2}{r^2} \tag{53}$$

Substitute the complex notations of $n(z)$, z and z_0 into the right-hand side of the first equation of (15):

$$\frac{\overline{n(z)}}{\overline{z-z_0}} = \frac{n_1-in_2}{dx-idy} = \frac{(n_1-in_2)(dx+idy)}{(dx)^2 + (dy)^2} = \frac{n_1dx + n_2dy + i(n_1dy - n_2dx)}{(dx)^2 + (dy)^2} \tag{54}$$

Compare (53) and (54), the first equation in (15) is proved.

Second Equation:
For the second equation of (15), we can use the similar procedure.

$$\frac{\cos\beta}{r} = -\frac{\vec{r}\cdot\vec{\xi}}{r^2} = -\frac{dx\cdot\xi_1 + dy\cdot\xi_2}{r^2}$$

$$\frac{\overline{\xi(z_0)}}{\overline{z-z_0}} = \frac{\xi_1-i\xi_2}{dx-idy} = \frac{(\xi_1-i\xi_2)(dx+idy)}{(dx)^2 + (dy)^2} = \frac{\xi_1dx + \xi_2dy + i(\xi_1dy - \xi_2dx)}{(dx)^2 + (dy)^2}$$

We can see

$$\frac{\cos\beta_0}{r} = -\frac{\vec{r}\cdot\vec{\xi}}{r^2} = -Re\left\{\frac{\overline{\xi(z_0)}}{\overline{z-z_0}}\right\}$$

Third Equation:
To prove the third equation of (15), we just directly substitute the complex notations of $n(z)$ and $\xi(z_0)$ to have:

$$Re\{n(n)\cdot\overline{\xi(z_0)}\} = Re(n_1 + in_2)(\xi_1-i\xi_2) = Re\{n_1\xi_1 - n_2\xi_2 + i(\xi_1n_2 - \xi_2n_1)\}$$

$$= n_1\xi_1 + n_2\xi_2 \vec{n}\cdot\vec{\xi} = \cos\varphi_0$$

Fourth Equation:
The left-hand side of the fourth equation can be expanded as:

$$\frac{(2\cos\beta\cos\beta_0 + \cos\varphi_0)}{r^2} = \frac{(2r\cos\beta\cdot r\cos\beta_0 + r^2\cos\varphi_0)}{r^4}$$

$$= \frac{-2(dx\cdot n_1 + dy\cdot n_2)(dx\cdot\xi_1 + dy\cdot\xi_2) + ((dx^2 + (dy)^2))(n_1\cdot\xi_1 + n_2\cdot\xi_2)}{r^4}$$

$$= \frac{-(dx)^2\xi_1 \cdot n_1 - (dy)^2\xi_2 \cdot n_2 - 2dxdy \cdot n_1 \cdot \xi_2 - 2dxdy \cdot n_2 \cdot \xi_1 + (dx)^2 n_2 \cdot \xi_2 + (dx)^2 n_2 \cdot \xi_1}{r^4}$$

$$= -\frac{(dxn_1 + dyn_2)(dx\xi_1 + dy\xi_2) - (dyn_1 - n_2 dx)(dy\xi_1 - \xi_2 dx)}{r^4}$$

The right-hand side of fourth equation is:

$$\frac{\overline{n(z)}\xi(z_0)}{(\overline{z-z_0})^2} = \frac{(z-z_0)^2 \overline{n(z)}\xi(z_0)}{(z-z_0)^2 (\overline{z-z_0})^2} = \frac{(z-z_0)\overline{n(z)}(z-z_0)\overline{\xi(z_0)}}{r^4}$$

$$= \frac{(dx+idy)(n_1-in_2)(dx+idy)(\xi_1-\xi_2)}{r^4}$$

$$= \frac{(dxn_1 + dyn_2 + idyn_1 - in_2 dx)(dx\xi_1 + dy\xi_2 + idy\xi_1 - i\xi_2 dx)}{r^4}$$

Consider the real part of above equation:

$$Re\left\{\frac{\overline{n(z)}\xi(z_0)}{(\overline{z-z_0})^2}\right\} = \frac{(dxn_1 + dyn_2)(dx\xi_1 + dy\xi_2) - (dyn_1 - n_2 dx)(dy\xi_1 - \xi_2 dx)}{r^4}$$

We obtain:

$$\frac{(2\cos\beta\cos\beta_0 + \cos\varphi_0)}{r^2} = -Re\left\{\frac{\overline{n(z)}\xi(z_0)}{(\overline{z-z_0})^2}\right\}$$

Fifth Equation:

We can use the first equation to help us to prove this last equation:

$$\cos 2\beta = 2\cos^2\beta - 1 = \frac{1}{2}\left(\frac{\overline{n(z)}}{\overline{z-z_0}} + \frac{n(z)}{z-z_0}\right)^2 (\overline{z-z_0})(z-z_0) - 1$$

$$= \frac{1}{2}\left(\frac{\overline{n(z)}^2}{(\overline{z-z_0})^2} + 2\frac{\overline{n(z)}}{\overline{z-z_0}}\frac{n(z)}{z-z_0} + \frac{n(z)^2}{(z-z_0)^2}\right)(\overline{z-z_0})(z-z_0) - 1$$

$$= \frac{1}{2}\frac{\overline{n(z)}^2}{(\overline{z-z_0})}(z-z_0) + \frac{1}{2}\frac{n(z)^2}{(z-z_0)}(\overline{z-z_0})$$

$$= Re\left\{\frac{z-z_0}{\overline{z-z_0}}\overline{n^2(z)}\right\}$$

Thus, all the results in Eq. (15) are verified.

References

[1] Stern M. A general boundary integral formulation for the numerical solution of plate bending problems. Int J Solids Struct 1979;15:769–82.

[2] Morjaria M, Mukherjee S. Inelastic analysis of transverse deflection of plates by the boundary element method. J Appl Mech 1980;47:291.

[3] Tanaka M. Integral equation approach to small and large displacements of thin elastic plate. In: Brebbia CA, editor. Proceedings of the fourth international seminar on boundary element methods in engineering. Southampton, England: Springer-Verlag; 1982. p. 526.

[4] Kamiya N, Sawaki Y. An integral equation approach to finite deflection of elastic plates. Int J Nonlinear Mech 1982;17:187–94.

[5] Stern M. Boundary integral equations for bending of thin plates". In: Brebbia CA, editor. Progress in boundary elements. London: Pentech Press; 1983 [chapter 6].

[6] Liu YJ. Finite deflection analysis of thin elastic plate by the boundary integral equation method, M.S. Thesis, Aerospace Engineering Department, Northwestern Polytechnical University, 1984 [in Chinese].

[7] Ye TQ, Liu YJ. Finite deflection analysis of elastic plate by the boundary element method. Appl Math Modelling 1985;9:183–8.

[8] Hartmann F, Zotemantel R. The direct boundary element method in plate bending. Int J Numer Methods Eng 1986;23:2049–69.

[9] Liu YJ. Elastic stability analysis of thin plate by the boundary element method—a new formulation. Eng Anal Boundary Elem 1987;4:160–4.

[10] Beskos DE, editor. Boundary Element analysis of plates and shells. Berlin: Springer-Verlag; 1991.

[11] Aliabadi MH. The boundary element method.Applications in solids and structures, vol. 2. Chichester: Wiley; 2002.

[12] Greengard LF. The rapid evaluation of potential fields in particle systems. Cambridge: The MIT Press; 1988.

[13] Greengard LF, Rokhlin V. A fast algorithm for particle simulations. J Comput Phys 1987;73:325–48.

[14] Rokhlin V. Rapid solution of integral equations of classical potential theory. J Comput Phys 1985;60:187–207.

[15] Nishimura N. Fast multipole accelerated boundary integral equation methods. Appl Mech Rev 2002;55:299–324.

[16] Liu YJ, Mukherjee S, Nishimura N, Schanz M, Ye W, Sutradhar A, et al. Recent advances and emerging applications of the boundary element method. Appl Mech Rev 2011;64:1–38.

[17] Liu YJ, Nishimura N. The fast multipole boundary element method for potential problems: a tutorial. Eng Anal Boundary Elem 2006;30:371–81.

[18] Liu YJ. Fast multipole boundary element method—theory and applications in engineering. Cambridge: Cambridge University Press; 2009.

[19] Greenbaum A, Greengard L, Mayo A. On the numerical solution of the biharmonic equation in the plane. Physica D 1992;60:216–25.

[20] Greengard LF, Kropinski MC, Mayo A. Integral equation methods for Stokes flow and isotropic elasticity in the plane. J Comput Phys 1996;125:403–14.

[21] Gumerov NA, Duraiswami R. Fast multipole method for the biharmonic equation in three dimensions. J Comput Phys 2006;215:363–83.

[22] Gao X-W. The radial integration method for evaluation of domain integrals with boundary-only discretization. Eng Anal Boundary Elem 2002;26:905–16.

[23] Partridge PW, Brebbia CA, Wrobel LC. The dual reciprocity boundary element method. Southampton: Computational Mechanics Publications; 1992.

[24] Saad Y, Schultz M. A generalized minimal residual algorithm for solving nonsymmetric linear system. SIAM Journal Sci Stat Comput 1986;7:856–69.

[25] Timoshenko SP, Woinowsky-Krieger S. Theory of plates and shells. 2nd ed New York: McGraw-Hill; 1987.

[26] Meijers P. Doubly-periodic stress distributions in perforated plates, Thesis, Delft University,1967.

[27] O'Donnell WJ. Effective elastic constants for the bending of thin perforated plates with triangular and square penetration patterns. J Eng Ind 1973;95: 121–8.

[28] Lee J-K, Kim J-G. An analytical study on prediction of effective elastic constants of perforated plate. J Mech Sci Technol 2005;19:2224–30.

[29] Bebendorf M. Hierarchical matrices: a means to efficiently solve elliptic boundary value problems. Berlin: Springer-Verlag; 2008.

[30] Rjasanow S, Steinbach O. The fast solution of boundary integral equations. Berlin: Springer; 2007.